Impact Behavior and Fracture Morphology of Acrylonitrile–Butadiene–Styrene Resins Toughened by Linear Random Styrene–Isoprene–Butadiene Rubber

Juan Yang,[1,2] Chao-Xian Wang,[2] Zhi-Sheng Yu,[3] Yang Li,[3] Ke-Ke Yang,[1] Yu-Zhong Wang[1]

[1]*Center for Degradable and Flame-Retardant Polymeric Materials, College of Chemistry, State Key Laboratory of Polymer Materials Engineering, National Engineering Laboratory of Eco-Friendly Polymeric Materials (Sichuan), Sichuan University, Chengdu 610064, China*
[2]*Research Institute, Beijing Yanshan Petrochemical Company, Beijing 102500, China*
[3]*Department of Polymer Science and Engineering, School of Chemical Engineering, Dalian University of Technology, Dalian 116012, China*

Received 11 August 2010; accepted 22 November 2010
DOI 10.1002/app.33773
Published online 21 March 2011 in Wiley Online Library (wileyonlinelibrary.com).

ABSTRACT: A novel toughening modifier, styrene–isoprene–butadiene rubber (SIBR), was used to improve the impact resistance and toughness of acrylonitrile–butadiene–styrene (ABS) resin via bulk polymerization. For comparison, two kinds of ABS samples were prepared: ABS-1 was toughened by a conventional modifier (a low-cis polybutadiene rubber/styrene–butadiene block copolymer), and ABS-2 was toughened by SIBR. The mechanical properties, microstructures of the as-prepared materials, and fracture surface morphology of the specimens after impact were studied by instrumented notched Izod impact tests and tensile tests, transmission electron microscopy, and scanning electron microscopy, respectively. The mechanical test results show that ABS-2 had a much higher impact strength and elongation at break than ABS-1. The microscopic results suggested that fracture resistance of ABS-1 only depended on voids, shear yielding, and few crazing, which resulted in less ductile fracture behavior. Compared with ABS-1, ABS toughened by linear random SIBR (ABS-2) displayed the synergistic toughening effect of crazing and shear yielding, which could absorb and dissipate massive energy, and presented high ductile fracture behavior. These results were also confirmed by instrumented impact tests. © 2011 Wiley Periodicals, Inc. J Appl Polym Sci 121: 2458–2466, 2011

Key words: fracture; plastics; rubber; toughness

INTRODUCTION

Acrylonitrile–butadiene–styrene (ABS) resin is a rubber-toughened polymer and provides a good balance between rigidity and elasticity. As a multiphase material, its properties are influenced by its morphology. In general, three major components generate a two-phase system in which the discrete rubber particles act as the dispersive phase and the poly(styrene-*co*-acrylonitrile) (SAN) copolymers act as the continuous phase in ABS.[1] As a result, ABS resin has great variety, and it is used widely in industrial fields.

As an important component of a rubber-toughened polymer, the dispersive rubber phase plays a significant role in toughening the ABS resin and can dissipate energy through the initiation of crazing and cavitation.[2] Therefore, the amount, structure, and types of rubber have a great effect on the properties of ABS resin. The most frequently used rubber is polybutadiene (PB).The performances of ABS toughened by PB rubber are affected by many important factors, such as the concentration of the rubber,[3,4] the size and the distribution of rubber particles,[1–5] the volume fraction of the rubber phase, and the degree of grafting.[1–6] In previous studies, we used lithium-catalyzed low-cis PB rubber (Li-700A), nickel-catalyzed high-cis PB rubber (Ni-9004), and their compounds to toughen ABS resins by bulk polymerization.[7,8] We found that the Li-700A/Ni-9004 compound promoted the formation of irregular, broadly distributed rubber particles with a salami structure, and the toughened product presented better mechanical properties. In addition, other rubber types have also been developed and used to toughen SAN copolymers for preparing ABS resin. Cavabaugh et al.[9] examined the effectiveness of different styrene–butadiene copolymers as interfacial agents in blends of polystyrene with PB and concluded that a long asymmetric diblock styrene–butadiene segment was the most effective compatibilizer. Steenbrink et al.[10] studied the toughening effect on the SAN matrix of acrylic core–shell rubber particles and pointed out that the mechanical properties of the rubber particles' core were the key to the toughening efficiency. However, there have been few pertinent reports on ABS resin toughened by a styrene–isoprene–butadiene

Correspondence to: Y.-Z. Wang (yzwang@scu.edu.cn).
Contract grant sponsor: National Science Foundation of China; contract grant number: 50933005.

terbasic adhesive. In general, a styrene–isoprene–butadiene rubber (SIBR) with a special molecular structure, such as linear random type or starlike block type, can be designed and synthesized by the anionic polymerization of styrene, isoprene, and butadiene. Because of its lower glass-transition temperature and main-chain microstructures involving cis-poly(1,4-butadiene) rubber (BR) and cis-polyisoprene rubber (IR), SIBR has the advantages of low-temperature resistance and excellent elasticity. Eventually, it can remarkably affect the morphology and properties of toughened ABS resins.

The modification made by rubber is aimed at improving the fracture toughness with slight or even no loss of other properties. Nowadays, the common method for characterizing the fracture resistance is the impact test, which only gives limited information in high-speed-fracture situations. The morphological study of the fracture surface of material may be helpful in explaining in detail how the rubber particles contribute to plastic deformation and fracture toughness. Many studies have elucidated the relation of impact toughness and fracture morphology. For example, Loyens and Groeninckx[11] studied the deformation mechanisms of rubber-toughened poly(ethylene terephthalate) with the fractography of impact fractured samples and tensile dilatometry and found that the ductile fracture behavior consisted of massive rubber cavitation and extensive matrix shear yielding. The high impact toughness and the toughening mechanism of polypropylene/$CaCO_3$ nanocomposites were studied by means of scanning electron microscopy (SEM) and instrumented falling-weight impact testing. The SEM micrographs of the impact-fractured surface and bulk morphology underneath the fracture surface of broken Izod samples, together with the results of the impact testing, suggested that the plastic deformation zone formed in the crack-initiation stage was responsible for the high impact toughness of the annealed nanocomposites.[12]

We carefully observed the impact-fracture morphologies of an ABS resin toughened by an SIBR elastomer (ABS-2) and a commercial product produced by bulk polymerization (ABS-1); we examined in detail the impact-fracture behavior of the toughened materials and found a correlation between the morphology and the impact-fracture mechanism. Possible reasons are also proposed to interpret the differences in the impact toughness behaviors of the synthesized resin and the commercial resin.

EXPERIMENTAL

Materials

Two ABS samples were used in this study. ABS-1 was an extrusion-grade commercial product prepared by continuous bulk polymerization and toughened with approximately 10 wt % compounded rubber (low-cis PB rubber/styrene–butadiene block copolymer). ABS-2 was made in the laboratory with approximately 12 wt % linear random SIBR as a toughening modifier. A detailed description of the polymerization can be found in our earlier articles.[7,8]

Mechanical testing

Tensile tests were conducted according to ISO-527 on an Instron 5567 universal material testing machine (Boston, USA) at 23°C with a crosshead speed of 5.0 mm/min, an initial gaze length of 40.0 mm, and a cross section of 4.0×2.1 mm^2. All tensile test specimens were injection-molded into a dumbbell shape.

The instrumented notched Izod impact tests were performed according to ISO-180 on a Ceast 695606 Resile Impact instrument (Pianezza, Italy) with a data acquisition unit (Ceast DAS 4000) and a maximum work capacity of 2.7 J. Data were acquired at a time interval of 1 μs per point. All impact test specimens were shaped with dimensions of $80.0 \times 10.0 \times 4.0$ mm^3. The notch was milled, having a depth of 2 mm and an angle of 45°, by means of a Ceast 6951 notching machine.

All of the testing specimens were prepared by an RR3400 model 2 injection test sample molding apparatus (Ray-Ran, Warwickshire, U.K.). The injection-molding parameters were as follows: melting temperature = 230°C, mold temperature = 90°C, holding pressure time = 60 s, and cooling time = 60 s. Before testing, the specimens were stored at 23°C at a relative humidity of 50% for at least 48 h after molding. For both the tensile and impact tests, five specimens were tested for each sample. The average of the five values was used in the subsequent analysis.

Fractography

In Figure 1, the shadow part presents the impact-fractured surface. Three different sites of impact-fractured surfaces were observed by SEM and transmission electron microscopy (TEM). The first site was as close as possible to the notch tip, the second was located at a distance of about 1.0 mm from the notch tip, and the third was located at a distance of about 2.0–2.5 mm from the notch tip.

The impact-fractured surface morphology was observed by a Quanta 200 scanning electron microscope (FEI) (Oregon, USA) with an operating voltage of 15 kV. All of the specimens were sputter-coated with gold to minimize electrostatic charging.

The morphology was observed by a TECNAI20 transmission electron microscope (FEI) (Oregon,

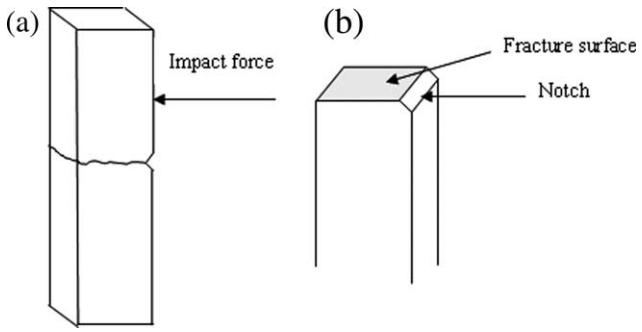

Figure 1 Schematic of the impact-fractured surface of a broken specimen.

USA) with an accelerating voltage of 200 kV. The TEM specimens were prepared by ultramicrotoming with a diamond knife on an ultramicrotome (Leica, Switzerland) at −120°C. The thickness of the section was less than 100 nm. The direction of the section was parallel to the impact-fractured surface. The sections were stained by exposure to osmium tetroxide vapors for 24 h.

RESULTS AND DISCUSSION

Mechanical properties

The data of the mechanical properties of the two ABS resins are summarized in Table I. Although ABS-2 had a 2% higher rubber content than ABS-1, we mainly put emphasis on the type rubber, not the others. Under the same test conditions, there was little difference in the tensile strength and breaking strength, but there was a distinct difference in the impact resistance between them. ABS-2 had a relatively high value of impact strength, 468.0 J/m, and ABS-1 had a relatively low value, 167.6 J/m. Obviously, ABS-2 could greatly improve the impact properties with little loss to other properties. The considerably great elongation at break of ABS-2 was ascribed to its ductility and flexibility of linear random SIBR chains. For ABS-1, because of the higher content of 1,2-isomers, more pendant double bonds existed on the macromolecular chains of low-cis PB and styrene–butadiene block copolymer, making its chains arrange loosely.[8] ABS-1 had a poorer elongation at break than ABS-2.

To compare the details of the impact fracture behavior of the ABS resins, the whole force–time curve should also be considered. Representative

TABLE I
Mechanical Properties of the ABS Resins

Code	Impact strength (J/m)	Tensile strength (MPa)	Break strength (MPa)	Elongation at break (%)
ABS-1	167.6	53.6	39.5	7.3
ABS-2	468.0	45.0	37.9	20.6

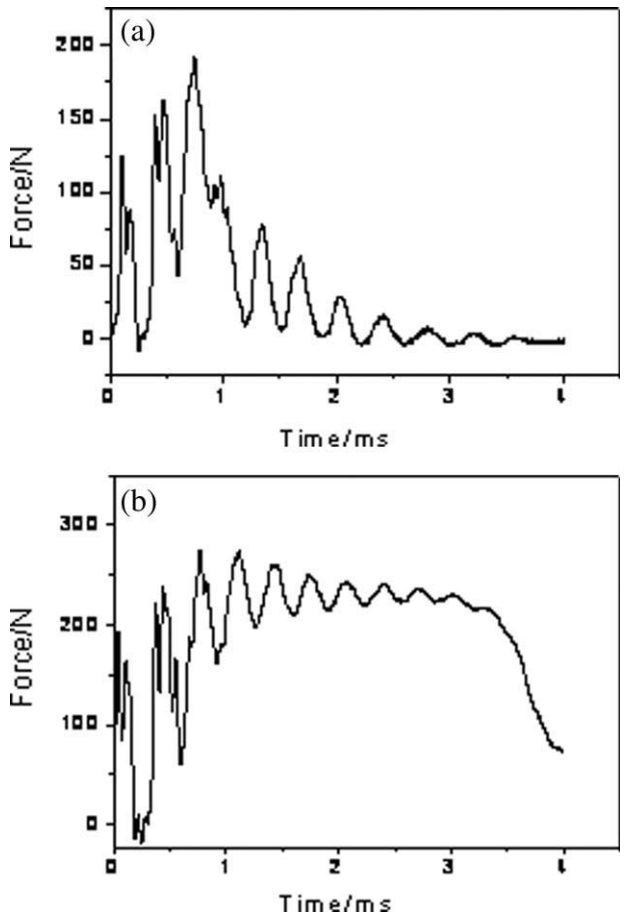

Figure 2 Force–time curves of ABS resins from the instrumented notched impact tests: (a) ABS-1 and (b) ABS-2.

force–time curves of the ABS resins are depicted in Figure 2. First, some related terms are interpreted.[13] The *peak force* (F_m) is the highest load and can also be presumed as a threshold beyond which the material fractures. It is assumed that crack initiation occurs at F_m. The *crack-initiation energy* is defined as the area under the force–time curve before F_m, and the *crack-propagation energy* is defined as that after F_m. T_m is the time corresponding to F_m. The conventional total breaking energy is the total fracture energy absorbed during the test and is represented by the area under the force–time curve. As a result, the fracture energy not only is dissipated in the crack-initiation stage but is also required for the crack-propagation stage.

As depicted in Figure 2(a), the force–time curve of ABS-1 was nonlinear and sawtooth trace. The impact force increased up to a maximum value and dropped abruptly at one particular point to zero. Because fracture is a result of the crack-initiation and crack-propagation processes, a certain amount of energy must be provided during the crack-initiation and crack-propagation stages. From Figure 2(a), we can presume that the most energy was consumed in the crack-initiation stage, whereas little energy was dissipated in the crack-propagation stage of ABS-1.

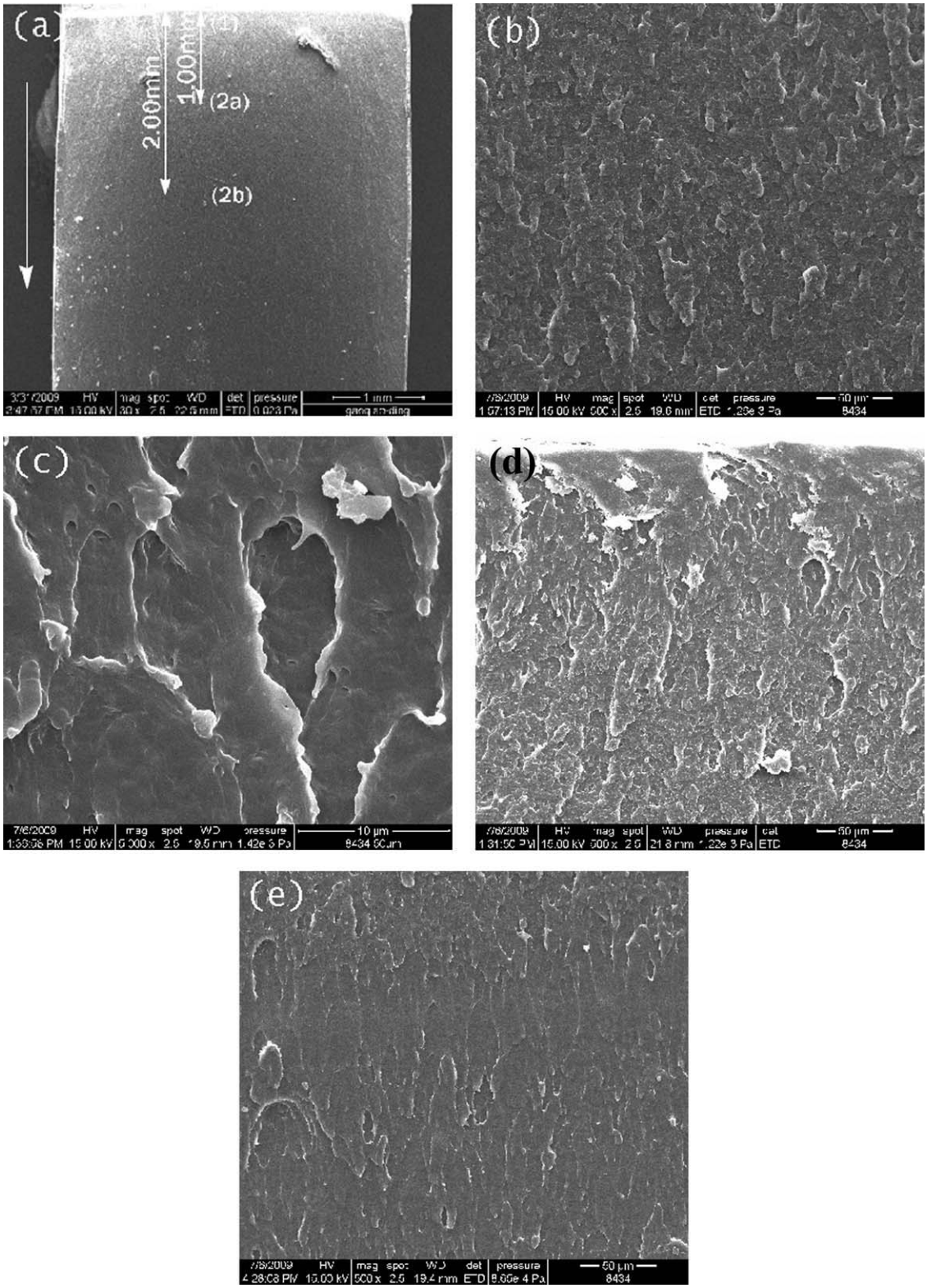

Figure 3 SEM micrographs of the impact-fractured surface of ABS-1: (a) the impact-fractured surface, (b) the area near the notch tip, (c) the area near the notch tip at a higher magnification, (d) the area approximately 1.0 mm away from the notch root and (e) the area approximately 2.0 mm away from the notch root.

The force–time curve of ABS-2 was still nonlinear and sawtooth trace, but it showed a different fracture behavior. As shown in Figure 2(b), the impact force dropped slowly after the maximum value that was reached, and there was not a definitive point where the crack initiation started or the crack-initiation process stopped.[14] ABS-2 could sustain a fracture force of about 274.0 N for a few milliseconds;

this indicated a higher force needed to initiate a real crack. In addition, the crack-propagation time for ABS-2 was much longer than that of ABS-1; the slowly propagating crack demonstrated a larger amount of fracture energy in the crack-propagation stage of ABS-2. ABS-2 could dissipate and absorb more energy than ABS-1. So the crack-propagation energy could not be neglected compared with the total energy. This also suggests that the higher toughness of the ABS-2 was due to the higher energy absorption during the entire fracture process.

Fracture characteristics of the ABS resins

Fracture morphology (SEM)

Because fracture is a complex process, the details of fracture information were obtained by SEM. The crack-propagation direction is indicated with an arrow in the micrograph. Representatives SEM micrographs of the fracture morphology of ABS resins are presented in Figures 3 and 4, respectively. First, the fracture characteristics of ABS-1 are described as follows. Figure 3(a) presents the fracture surface of the ABS-1 impact testing specimens. The fracture surface could be divided into different regions. The crack propagated from up to down. As shown in Figure 3(a), two regions could be defined as the crack-initiation region (region 1) and the crack-propagation region (region 2), respectively. The latter region could be further divided into two subregions (A and B) according to the different modes of crack propagation.

The crack-initiation region (region 1) near the notch tip was a smaller zone compared with the crack-propagation region (region 2). The surface of region 1 appeared to be less ductile feature, as shown in Figure 3(b). In this region, there were some circular marks of void formation. Some microvoids were formed by the coalescence of neighboring voids, as shown in Figure 3(c) at a higher magnification. It was clear that the void coalescence in front of the initial crack constituted the initiation of fracture, and the plastic deformation implied that shear yielding took place in the SAN matrix. In a word, the region around the notch tip consisted of a plastic region where crack initiation occurred, and a certain amount of energy was absorbed.

In addition, the crack-propagation region (region 2A) was about 1.0 mm away from the notch tip and was brittlelike with distributed small vein-type features [Fig. 3(d)]. In this zone, the size of circular marks seemed to decrease as the distance from the notch tip increased. Also, some fibrils and signs of ductile tearing were easily observed on the fracture surface. These features indicate that the rate of crack propagation was so high that the material had no adequate time to respond and restrict the occurrence of fracture. Region 2B was about 2.0 mm away from the notch tip and displayed the stick–slip feature, as shown in Figure 3(e). This feature may be represented as the stay–develop crack-propagation process, accompanied with the relaxation of stress.[15] This implied that instability of the crack propagation occurred when the increment of the crack grew rapidly. As shown in Figure 3(d,e), the fracture surface presented brittlelike behavior, which led to less energy absorbed during the crack-propagation process.

The micrographs of the fracture surface of ABS-2 were also studied. The crack propagated from up to down. The fracture surface was still divided into two regions; this showed obvious ductilelike behavior, as shown in Figure 4(a). However, the fracture surface morphologies of the two regions were distinctly different from those of ABS-1. An intensive plastic deformation in ABS-2 occurred; this revealed a more ductile mode than ABS-1. The differences in the morphology of materials tended to account for the obvious differences in their impact strength obtained in the impact tests. Figure 4(b) shows much more widespread shear deformation in region 1, just ahead of the notch tip. Such morphology was consistent with the more ductile fracture surface. In this region shown in Figure 4(b), the fracture surface was very rough overall with many extending conical marks (parabola, hyperbola, or ellipse); these represent the intersection point between the front of the primary cracks and the secondary cracks and, to a certain extent, exhibit a crack-branching effect. They also represent the level difference between the main fracture plane and the secondary fracture plane. If the secondary front propagates more slowly than the primary front, an ellipse is generated.[16] As shown at a higher magnification in Figure 4(c), microdrawing was observed on the fracture surface; this indicated that this zone had extensive deformation.

As shown in Figure 4(d), in region 2A, about 1.0 mm away from the notch tip, severe conical marks were still identified clearly, and the fibrils were produced extensively. In ABS-1, the rapid breakdown of crack propagation did not provide adequate time for the material to respond; this resulted in a brittlelike fracture behavior. By comparison, ABS-2 possessed a more ductile and rougher fracture surface and showed a slower breakdown of the crack-propagation region. The reason was possibly that the polymeric chain segments of SIBR provided more mobility and contributed a greater percentage elongation to the fracture of the ABS-2 material. This yielding region of the matrix absorbed more energy during the deformation process. In region 2B, about 2.5 mm away from the notch tip [Fig. 4(e)], it showed the chevron marking. The severity of the plastic

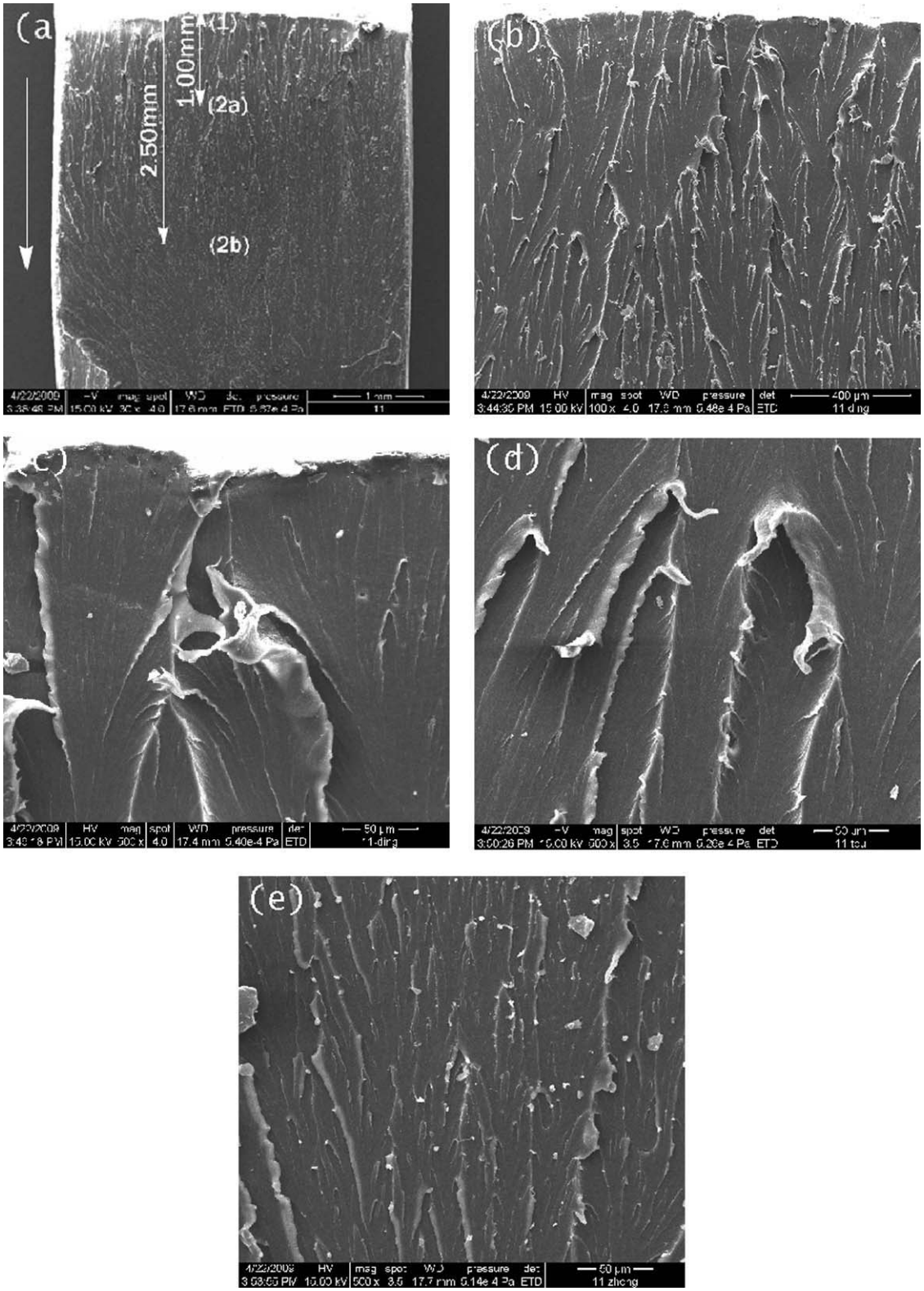

Figure 4 SEM micrographs of the impact-fractured surface of ABS-2: (a) the impact-fractured surface, (b) the area near the notch tip, (c) the area near the notch tip at a higher magnification, (d) the area approximately 1.0 mm away from the notch root, and (e) the area approximately 2.5 mm away from the notch root.

deformation decreased, and the extent of shear deformation diminished; that is, an accelerated speed of crack propagation was reached, and the rubber particles no longer effectively restricted the crack from growing. All in all, the aforesaid fracture surface morphology accounted for the fact that the

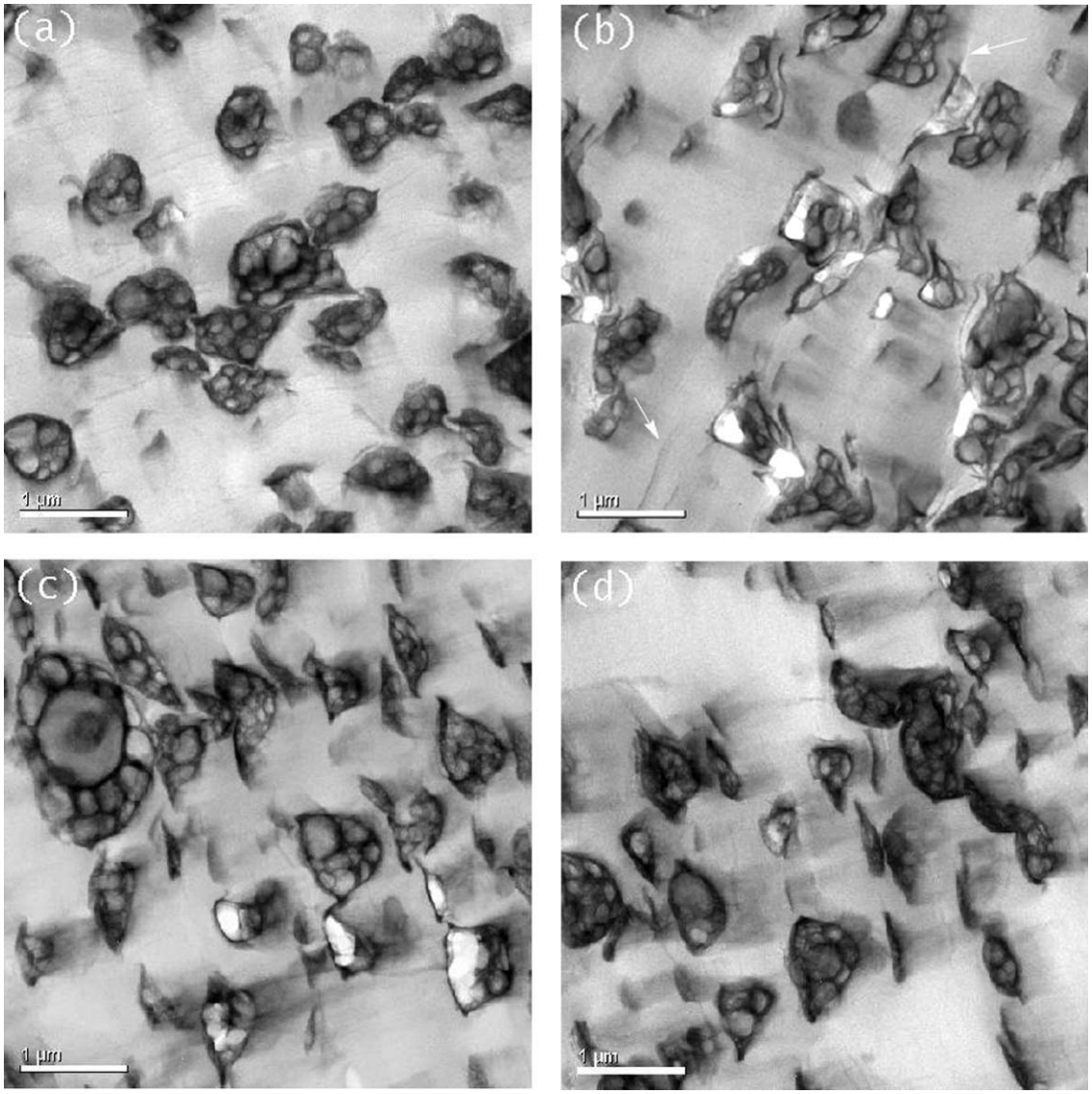

Figure 5 TEM micrographs of ABS-1: (a) the undeformed specimen before impact, (b) the area near the notch tip, (c) the area approximately 1.0 mm away from the notch root, and (d) the area approximately 2.0 mm away from the notch root.

fracture resistance of ABS-2 was much higher than that of ABS-1.

Microdeformation mechanisms (TEM)

To search for additional information on the fracture behavior of ABS resins, TEM observations were made on ultrathin sections from the impact-fractured surface. Typical TEM micrographs of the ABS resins are shown in Figures 5 and 6, respectively. We first depict the fracture characteristics of ABS-1. A TEM micrograph of an undeformed ABS-1 specimen before the impact test is given in Figure 5(a), which shows well-dispersed rubber particles with a salami structure with SAN occlusions. The average rubber particle size of ABS-1 from the statistics of a mass of micrographs was about 0.7 μm.

In Figure 5(b), the TEM observations in region 1 corresponds to the initial notch tip of ABS-1. The micrograph shows very little short black or bright lines in the matrix. There was no doubt that the lines were crazing, which was adjacent to the rubber particles.[17] As indicated in parts of Figure 5(b) by an arrow, the minute crazing generated from the rubber particle surface had the typical microstructures and the same internal details of draw fibrils; also, some of the crazing fibrils were broken down. These results indicate that the crazing developed in the matrix before the fracture occurred, and the crack was initiated by the coalescence of the crazing at this region. Moreover, the cavitation of rubber particles was also visible, and shear deformation was inferred from the distortion of the rubber particles. On the basis of other researchers' previous studies, the cavitation occurred first and could then induce the shear yielding taking place.[18,19] Sequential shearing and stretching progress combined with voiding

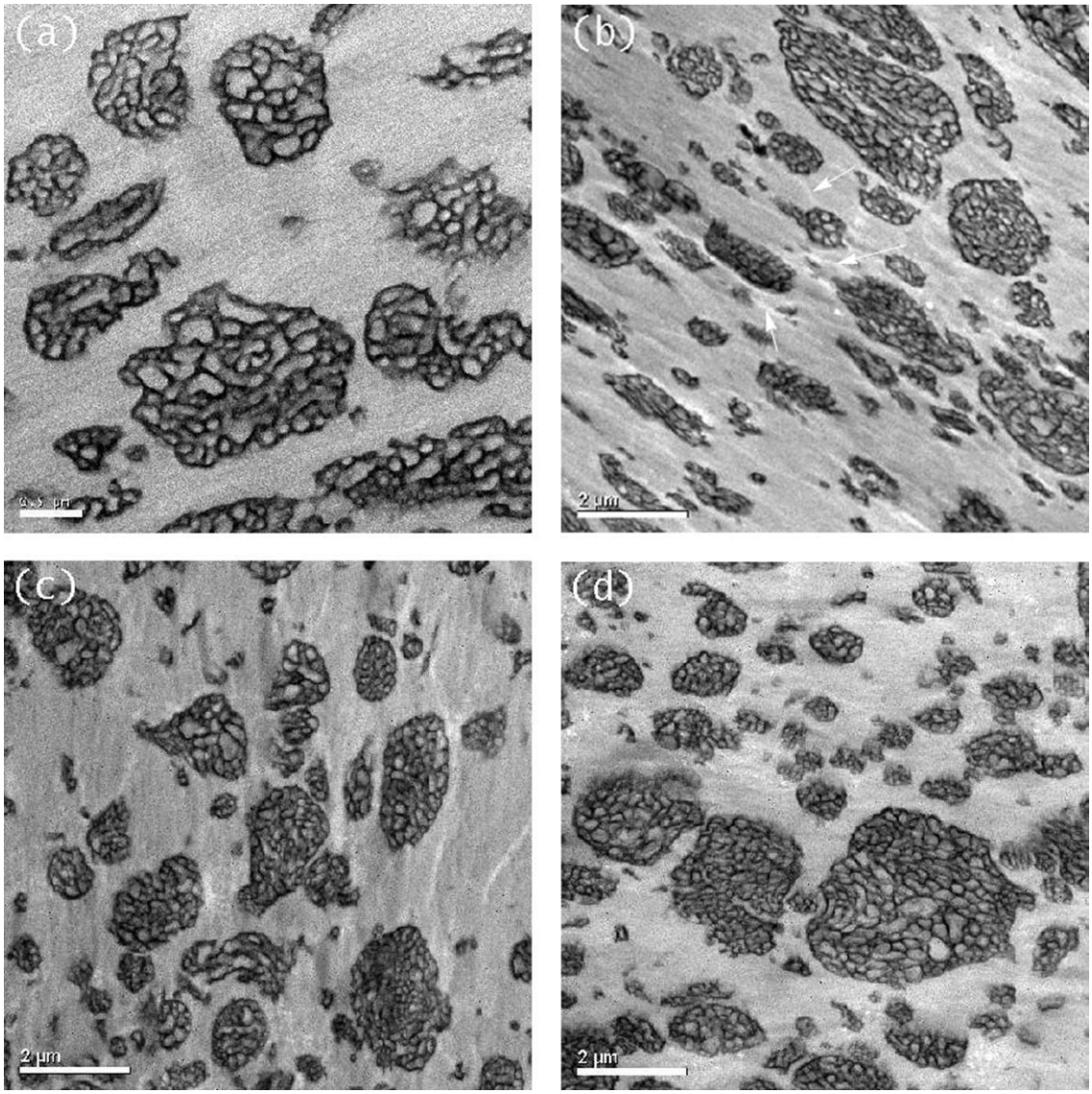

Figure 6 TEM micrographs of ABS-2: (a) the undeformed specimen before impact, (b) the area near the notch tip, (c) the area approximately 1.0 mm away from the notch root, and (d) the area approximately 2.5 mm away from the notch root.

could obviously dissipate the impact energy on the material before fracture occurred.

As shown in Figure 5(c), there were few crazes in the region 2A, away from the notched tip by about 1.0 mm. Some voids were formed inside the rubber particles, and the cavitation was evident throughout the region because void formation could facilitate to the shearing yielding formation, which was still discovered in the region. Some rubber particles deformed with teardrop shape were ascribed to the apparent shear yielding of the SAN matrix. However, in the region 2B [Fig. 5(d)], the rubber particles were slightly elongated and distorted along a certain direction. Meanwhile, there were fewer voids and crazing in the SAN matrix. Few cavities formed were due to good interfacial adhesion between the two phases.

The morphology shown in Figure 5 may support the results of SEM observation. We deduced that the fracture behavior of ABS-1 only depended on the generation of voids, shear yielding, and a few crazes contributing to energy absorption. However, these could not absorb much more energy and resulted in a less ductile fracture behavior.

Moreover, the typical TEM micrographs of ABS-2 shown in Figure 6 illustrated the deformation of the impact fracture process. In Figure 6(a), the undeformed ABS-2 specimen is shown. The average size of its rubber particles was about 1.1 μm. The occlusions in the rubber particles were much larger, and the rubber–occlusion interfaces became more clear. The difference was attributed to the different rubber types. PB and polyisoprene segments of SIBR were capable of insetting in the SAN matrix; this led to a different grafting extent of the SIBR-*graft*-SAN chains. The grafting extent influenced the dispersion of the rubble particles in the matrix.[20] This indicated

that the special rubber type changed the internal structure of rubber particles, which was beneficial for the rubble particle modulus. On the one hand, because the volume of the SAN occlusion in the rubber particles enlarged the size of the rubber particles to some extent, the average rubber particle size of ABS-2 was larger than that of ABS-1. On the other hand, the graft copolymers with a higher number of branches reduced more of the interfacial tension between the SAN matrix and rubber phase and stabilized the interface better. Meanwhile, the polystyrene segments of SIBR had good compatibility with the matrix; this favored the increase in the interfacial strength of the rubber particles and SAN matrix. Any increase in the adhesion energy added to the fracture energy of the material. This was consistent with the results of the instrumented impact tests; the absorbed energy of ABS-2 in impact fracture testing was proven to increase evidently.

As indicated by the arrow in Figure 6(b), the micrograph provided clear evidence of multiple crazes in this region. Because the larger rubber particles initiated crazes much more easily than the smaller ones, both the craze opening width and the total number of crazes shown in Figure 6(b) were bigger and greater in number than those in Figure 5(b). A majority of rubber particles, and even the submicrometer ones (ca. 0.7 μm), seemed to be connected with one or multiple crazes. Crazing was initiated by both larger rubber particles and smaller rubber particles in the vicinity of larger rubber particles. Only the former acted as crazing terminator. Moreover, they extended like a bridge to bridge the independent small particles. Thus, it was the impact energy of ABS-2 that was required to form an extensive network of crazing. At the same time, we observed clearly that severe shear deformation occurred in this region, and considerable elongation and distortion of the rubber particles were also observed. Obviously, this morphology was sufficient to support the results of SEM observation. ABS-2 included a higher degree of shear yielding than ABS-1. Shearing and stretching combined deformation and the formation of macrocrazing obviously dissipated the impact energy and increased the impact resistance of ABS-2.

According to Figure 6(c), the micrograph still provided clear evidence of multiple crazes in region 2A of ABS-2. There were multiple crazes formed in the region, where each craze had a slightly smaller opening width; however, their number was much smaller than that in Figure 6(b). Also, the rubber particles were only partially elongated and distorted. The cracks proceeded continuously and were slowed down via deformation mode and eventually helped to increase the fracture energy. Figure 6(d), corresponding to region 2B, shows that most of the rubble particles maintained their spherical shape. There was almost no obvious elongation and distortion occurring in these rubble particles. The micrograph also suggests no crazing throughout this region.

Conclusively, when we consider the morphological characterization and the results of impact testing at the same time, we can explain the high ductile fracture behavior of ABS-2 as follows: the synergistic toughening effect of multiple crazes and shear yielding deformation was favorable to the absorption and dissipation of massive energy and resulted in a ductile fracture feature of the toughened material.

CONCLUSIONS

The fracture resistance of ABS-1 only depended on voids, shear yielding, and few crazes and resulted in less ductile fracture behavior. ABS toughened by linear random SIBR (ABS-2) displayed the synergistic toughening effect of multiple crazes and shear yielding; these could absorb and dissipate massive energy and presented a much higher ductile fracture behavior. The linear random SIBR could be used for special toughening materials as the new-style substrate for lower temperature applications and higher toughnesses.

References

1. Xu, X. F.; Yang, H. D.; Zhang, H. X. J Appl Polym Sci 2005, 98, 2165.
2. Okamoto, Y.; Miyagi, H.; Mitsui, S. Macromolecules 1993, 26, 6547.
3. Han, Y.; Lach, R.; Grellmann, W. J Appl Polym Sci 2001, 79, 9.
4. Keskkula, H.; Kim, H.; Paul, D. R. Polym Eng Sci 1990, 30, 1373.
5. Heckmann, W.; McKee, G. E.; Ramsteiner, F. Macromol Symp 2004, 214, 85.
6. Hasegawa, R.; Aoki, Y.; Doi, M. Macromolecules 1996, 29, 6656.
7. Yu, Z. S.; Li, Y.; Zhao, Z. F.; Wang, C. X.; Yang, J.; Zang, C. Q.; Li, Z. S.; Wang, Y. R. Polym Eng Sci 2009, 49, 2249.
8. Yu, Z. S.; Li, Y.; Wang, Y. R.; Yang, L.; Liu, Y.; Li, Y. T.; Li, Z. S.; Zhao, Z. F. Polym Eng Sci 2010, 50, 961.
9. Cavabaugh, T. J.; Buttle, K.; Turner, J. N.; Nauman, E. B. Polymer 1998, 39, 4191.
10. Steenbrink, A. C.; Litvinov, V. M.; Gaymans, R. J. Polymer 1998, 39, 4817.
11. Loyens, W.; Groeninckx, G. Polymer 2003, 44, 4929.
12. Lin, Y.; Chen, H. B.; Chan, C. M.; Wu, J. S. Macromolecules 2008, 41, 9204.
13. Lubert, W.; Rink, M.; Pavan, A. J Appl Polym Sci 1976, 20, 1107.
14. Dear, J. P. Polym Test 2000, 19, 569.
15. Yuan, Q.; Misra, R. D. K. Polymer 2006, 47, 4421.
16. Hartmann, B.; Lee, G. F. J Appl Polym Sci 1979, 23, 3639.
17. Kuboki, T.; Ben Yar, P. Y.; Takahashi, K.; Shinmura, T. Macromolecules 2000, 33, 5740.
18. Ramsteiner, F.; Heckmann, W.; McKee, G. E.; Breulmann, M. Polymer 2002, 43, 5995.
19. Parker, D. S.; Sue, H. J.; Huang, J.; Yee, A. F. Polymer 1990, 31, 2267.
20. Gao, G. H.; Zhou, C.; Yang, H. D.; Zhang, H. X. J Appl Polym Sci 2007, 103, 738.